JCTC Journal of Chemical Theory and Computation

Article

Cite This: J. Chem. Theory Comput. 2018, 14, 3071−3082

pubs.acs.org/JCTC

Green Functions and Self-Consistency: Insights From the Spherium Model

Pierre-François Loos,*[,†] Pina Romaniello,[‡,¶] and J. A. Berger[†,¶]

[†]Laboratoire de Chimie et Physique Quantiques, Université de Toulouse, CNRS, UPS, 31062 Toulouse, France

[‡]Laboratoire de Physique Théorique, Université de Toulouse, CNRS, UPS, 31062 Toulouse, France

[¶]European Theoretical Spectroscopy Facility (ETSF)

Supporting Information

ABSTRACT: We report an exhaustive study of the performance of different variants of Green function methods for the spherium model in which two electrons are confined to the surface of a sphere and interact via a genuine long-range Coulomb operator. We show that the spherium model provides a unique paradigm to study electronic correlation effects from the weakly correlated regime to the strongly correlated regime, since the mathematics are simple while the physics is rich. We compare perturbative GW, partially self-consistent GW and second-order Green function (GF2) methods for the computation of ionization potentials, electron affinities, energy gaps, correlation energies as well as singlet and triplet neutral excitations by solving the Bethe−Salpeter equation (BSE). We discuss the problem of self-screening in GW and show that it can be partially solved with a second-order screened exchange correction (SOSEX). We find that, in general, self-consistency deteriorates the results with respect to those obtained within perturbative approaches with a Hartree−Fock starting point. Finally, we unveil an important problem of partial self-consistency in GW: in the weakly correlated regime, it can produce artificial discontinuities in the self-energy caused by satellite resonances with large weights.

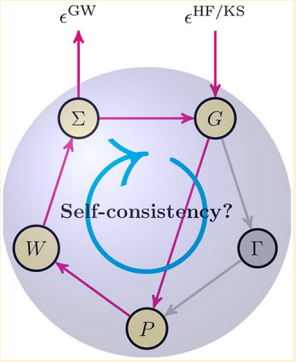

1. INTRODUCTION

The electronic structure of a many-body system is well characterized by its one-body Green function, G, since it provides several important physical properties of interest, for example, the total energy, the density, ionization potentials, electron affinities, as well as spectral functions, which are related to direct and inverse photoemission.[1−6] Formally, G is defined as an expectation value with respect to the ground-state wave function of the N-electron system.[7] Therefore, it is not useful in practical calculations. However, a closed set of equations yielding G, which does not require the explicit calculation of the ground-state wave function, was obtained by Hedin.[8] It connects the Green function, the irreducible vertex function Γ, the irreducible polarizability P, the dynamically screened Coulomb interaction W, and the self-energy Σ through a set of five integro-differential equations known as Hedin's equations (see also Figure 1)

$$G(12) = G_{\mathrm{H}}(12) + \int G_{\mathrm{H}}(13)\Sigma(34)G(42)\,\mathrm{d}(34) \tag{1a}$$

$$\Gamma(123) = \delta(12)\delta(13) + \int \frac{\delta\Sigma(12)}{\delta G(45)} G(46)G(75)\Gamma(673)\,\mathrm{d}(4567) \tag{1b}$$

$$P(12) = -i\int G(13)\Gamma(342)G(41)\,\mathrm{d}(34) \tag{1c}$$

$$W(12) = v(12) + \int v(13)P(34)W(42)\,\mathrm{d}(34) \tag{1d}$$

$$\Sigma(12) = i\int G(13)W(14)\Gamma(324)\,\mathrm{d}(34) \tag{1e}$$

where G_{H} is the one-body Hartree Green function, v is the bare Coulomb interaction, $\delta(12)$ is Dirac's delta function,[9] and 1 is a

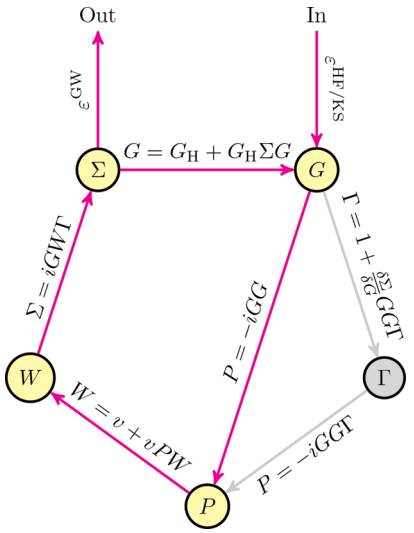

Figure 1. Hedin's pentagon.[8] The red path shows the self-consistent GW process which bypasses the computation of the vertex function Γ.

Received: March 12, 2018
Published: May 10, 2018

DOI: 10.1021/acs.jctc.8b00260
J. Chem. Theory Comput. 2018, 14, 3071−3082

composite coordinate gathering spin, space, and time variables $(\sigma_1, \mathbf{r}_1, t_1)$.

A particularly successful approximation to Hedin's equations in electronic-structure calculations is the so-called GW approximation,[8] which bypasses the calculation of the vertex corrections by setting[1−4] (see also Figure 1):

$$\Gamma(123) = \delta(12)\delta(13) \tag{2}$$

Historically, GW methods have been mostly applied to solids.[1,2] However, studies on atoms and molecules have been flourishing in the past ten years.[10−26] Nowadays, efficient implementations of GW methods for localized basis sets are available in several software, such as FIESTA,[4,10] MOLGW,[15] TURBOMOLE,[27−30] FHI-AIMS,[31−34] and others.

There exists many flavours of GW. The simplest and most popular variant is perturbative GW or G_0W_0,[35,36] which has been widely used in the literature to study solids, atoms and molecules.[12,13,22,23] Although G_0W_0 provides accurate results (at least for weakly/moderately correlated systems), it is strongly starting-point dependent due to its perturbative nature, and violates some important conservation laws, such as the conservation of energy, momentum and particle number.[37−39] Improvements may be obtained via partial self-consistency while the conservation laws are satisfied at full self-consistency.

However, things are not that simple, as self-consistency and vertex corrections are known to cancel to some extent.[40] Indeed, there is a long-standing debate about the importance of partial and full self-consistency in GW.[31−34,41−45] In some situations, it has been found that self-consistency can worsen spectral properties compared to the simpler G_0W_0 method. A famous example has been provided by the calculations performed on the uniform electron gas,[46−49] a paradigm central to many areas of physics and chemistry.[50] This was further evidenced in real extended systems by several authors.[51−54] However, other approximations may have caused such deterioration, for example, pseudopotentials[55] or finite-basis set effects.[56] These studies have cast doubt on the importance of self-consistent schemes within GW, at least for solid-state calculations. For finite systems, such as atoms and molecules, the situation is less controversial, and partially or fully self-consistent GW methods have shown great promise.[4,10,11,20,31−34,44,57,58]

To test the importance of self-consistency one could compare to benchmark results obtained with high-level electronic structure calculations. Extensive and elaborate benchmark sets have been compiled in quantum chemistry for a long time,[59−62] but in the Green-function community, they are only slowly emerging.[14,22,23,63−68] Unfortunately, it is somewhat difficult to obtain reliable benchmark results for molecular systems because there are always inherent errors introduced by the one-electron basis set incompleteness, the pseudopotentials or additional numerical procedures, such as Fourier transforms or the resolution of the identity approximation. In that regard, exactly or very accurately solvable models have ongoing value and are valuable both for illuminating the physics of more complicated systems and for testing theoretical approaches.[69−74] Besides, they offer unparalleled mathematical simplicity, while retaining much of the key physics.[75−78] One such model consists of two electrons, interacting through the long-range Coulomb potential but confined to the surface of a sphere, whose radius R can be tuned to mimic weakly correlated systems ($R \ll 1$) or strongly correlated systems ($R \gg 1$).[75,79] This paradigm possesses a number of interesting features, but the one of relevance here is that, for such a system, it is possible to compute the exact or near-exact properties of the one-, two- and three-electron systems. Additionally, one can obtain, like in the Hubbard model, most of the quantities of interest analytically, and the electronic interaction is, unlike the Hubbard model, genuinely long-range. Therefore, the "two-electrons-on-a-sphere" model—dubbed "spherium" in the remaining of the paper—can be seen as a unique theoretical laboratory to test the performances of the different GW variants.

The spherium model has already been considered by Schindlmayr[80] within the simple G_0W_0 method. In particular, he reported analytical expressions for various quantities, such as the independent-particle Green function, the dynamically screened Coulomb interaction and the self-energy. He also studied the accuracy of G_0W_0 for the prediction of the HOMO−LUMO energy gap for various R values and provided a detailed analysis of the convergence behavior of the energy gap with respect to the size of the one-electron basis set.

Here, we propose to extend the analysis of Schindlmayr[80] to unveil some interesting properties of self-consistent GW methods. In particular, we compare G_0W_0, partially self-consistent GW and second-order Green function (GF2) methods for a wide range of properties including ionization potentials, electron affinities, energy gaps, correlation energies, as well as singlet and triplet neutral excitations, by solving the Bethe−Salpeter equation (BSE). We also study a perturbative and self-consistent version of a second-order screened exchange correction (SOSEX) to the GW self-energy, labeled as GW+SOSEX. We focus here on self-consistent schemes that are widely used and available, for example, through the software packages mentioned above. For this reason fully self-consistent GW is beyond the scope of this work. Finally, we note that spherium represents a challenging test for GW because of the small amount of screening in two-electron systems.

The paper is organized as follows: In section 2, we briefly review the GW equations for spherium. Section 3 provides details about our perturbative and self-consistent GW implementations, and gives the expression of the self-energy for GF2 and GW+SOSEX. We also report the expression of the BSE singlet/triplet excitations and various energy functionals. Results are reported and discussed in section 4. Finally, we draw our conclusions in section 5. Atomic units are used throughout.

2. TWO ELECTRONS ON A SPHERE

In this section, we briefly review the GW equations for the spherium model, which consists of two opposite-spin electrons restricted to remain on the surface of a sphere of radius R.[75−79,81−88] The Hamiltonian of the system is simply

$$\hat{H} = -\frac{\nabla_1^2 + \nabla_2^2}{2} + \frac{1}{r_{12}} \tag{3}$$

where

$$\nabla_i^2 = \frac{1}{R^2}\left(\frac{\partial^2}{\partial\theta_i^2} + \cot\theta_i\frac{\partial}{\partial\theta_i} + \frac{1}{\sin^2\theta_i}\frac{\partial^2}{\partial\phi_i^2}\right) \tag{4}$$

is the angular part of the Laplace operator for electron i and $r_{12} = |\mathbf{r}_1 - \mathbf{r}_2|$ is the distance between the two electrons i.e., the electrons interact Coulombically *through* the sphere. Note that

DOI: 10.1021/acs.jctc.8b00260
J. Chem. Theory Comput. 2018, 14, 3071−3082

we eschew the introduction of a positively charged background, which is equivalent to a trivial energy shift.

The Hartree−Fock (HF) orbitals of spherium are the normalized spherical harmonics $Y_{lm}(\theta, \phi)/R$, where $0 \le l \le L$, $-l \le m \le +l$, L is the maximum angular momentum of the one-electron basis set, and (θ,ϕ) are the polar and azimuthal angles, respectively. We will use this convenient, orthogonal and complete basis set to represent the various quantities associated with GW methods. Moreover, because we focus our attention on the totally symmetric singlet ground state, all the quantities of interest are independent of m. Therefore, from here on, we drop the m dependence.[75] A crucial point here is that, as shown by Schindlmayr,[80] all the quantities reported in this section have a diagonal representation, that is, only their diagonal elements are nonzero. As we shall see below, this yields important simplifications in the GW equations and their implementation.

The HF orbital energies are given by

$$\epsilon_l^{\mathrm{HF}} = \frac{l(l+1)}{2R^2} + \frac{2}{R} + \Sigma_l^{\mathrm{x}} \tag{5}$$

where the exchange part of the self-energy is

$$\Sigma_l^{\mathrm{x}} = -\frac{1}{(2l+1)R} \tag{6}$$

Within the single-determinant approximation, in its singlet ground state, the lowest s-type spherical harmonic $Y_{00}(\theta,\phi)$ is doubly occupied and the electron density is uniform over the sphere[83]

$$\rho = 2\,|Y_{00}(\theta, \phi)/R|^2 = \frac{1}{2\pi R^2} \tag{7}$$

All the GW calculations reported in this study have been performed with a HF starting point.

As derived by Schindlmayr,[80] the independent-particle Green function is

$$G_l(\omega) = \frac{\delta_{0l}}{\omega - \epsilon_l - i\eta} + \frac{1-\delta_{0l}}{\omega - \epsilon_l + i\eta} \tag{8}$$

(where η is a positive infinitesimal and $\delta_{l_1 l_2}$ is the Kronecker delta[9]) and the polarizability function reads

$$P_l(\omega) = \frac{1-\delta_{0l}}{2\pi R^2}\left(\frac{1}{\omega - \Delta\epsilon_l + i\eta} - \frac{1}{\omega + \Delta\epsilon_l - i\eta}\right) \tag{9}$$

with

$$\Delta\epsilon_l = \epsilon_l - \epsilon_0 \tag{10}$$

Defining

$$W_l(\omega) = v_l + W_l^{\mathrm{c}}(\omega) \tag{11}$$

with

$$v_l = \frac{4\pi}{2l+1}R \tag{12}$$

the correlation part of the dynamically screened Coulomb interaction is

$$W_l^{\mathrm{c}}(\omega) = \frac{(1-\delta_{0l})v_l^2}{2\pi R}\frac{\Delta\epsilon_l}{\Omega_l}\left(\frac{1}{\omega - \Omega_l + i\eta} - \frac{1}{\omega + \Omega_l - i\eta}\right) \tag{13}$$

where

$$\Omega_l = \sqrt{\Delta\epsilon_l(\Delta\epsilon_l - 4\Sigma_l^{\mathrm{x}})} \tag{14}$$

are the (singlet) random phase approximation (RPA) excitation energies. Defining, respectively, the bare and screened two-electron integrals as

$$(l_1 l_2 l) = \frac{1}{R}\sqrt{\frac{v_{l_2}}{v_{l_1}}}\begin{pmatrix} l_1 & l_2 & l \\ 0 & 0 & 0 \end{pmatrix} \tag{15a}$$

$$[l_1 l_2 l] = \sqrt{\frac{\Delta\epsilon_{l_2}}{\Omega_{l_2}}}\,(l_1 l_2 l) \tag{15b}$$

this yields

$$\Sigma_l^{\mathrm{GW}}(\omega) = \frac{2(1-\delta_{0l})[0ll]^2}{\omega - \epsilon_0 + \Omega_l - i\eta} + \sum_{l_1 l_2 = 1}^{L} \frac{2[l_1 l_2 l]^2}{\omega - \epsilon_{l_1} - \Omega_{l_2} + i\eta} \tag{16}$$

for the correlation part of the GW self-energy, where

$$\begin{pmatrix} l_1 & l_2 & l \\ 0 & 0 & 0 \end{pmatrix}^2 = \sqrt{\frac{4\pi}{(2l_1+1)(2l_2+1)(2l+1)}} \times \int_0^{2\pi}\int_0^{\pi} \Upsilon_{l_1 0}(\theta,\phi)\Upsilon_{l_2 0}(\theta,\phi)\Upsilon_{l 0}(\theta,\phi)\sin\theta\,\mathrm{d}\theta\,\mathrm{d}\phi \tag{17}$$

defines the Wigner 3j symbol.[9] More details about the derivation of all these quantities can be found in ref 80.

3. GREEN FUNCTION METHODS

3.1. G_0W_0. In G_0W_0, one only updates once the orbital energies, which are obtained by solving a linearized (static) version of the quasiparticle equation[35,36]

$$\epsilon_l^{\mathrm{G_0W_0}} = \epsilon_l^{\mathrm{HF}} + Z_l(\epsilon_l^{\mathrm{HF}})Re[\Sigma_l^{\mathrm{GW}}(\epsilon_l^{\mathrm{HF}})] \tag{18}$$

where ϵ_l^{HF} and Σ_l^{GW} are given by eqs 5 and 16, respectively, and the renormalization factor

$$Z_l(\omega) = \left[1 - \frac{\partial Re[\Sigma_l^{\mathrm{GW}}(\omega)]}{\partial\omega}\right]^{-1} \tag{19}$$

specifies the weight of the quasiparticle energy in the spectral function

$$S_l(\omega) = \pi^{-1}|Im[G_l(\omega)]| \tag{20}$$

3.2. Self-Consistent GW. As mentioned in section 1, the major drawback of G_0W_0 is its starting point dependency. One way of getting rid of this shortcoming is to iterate the GW quantities until self-consistency has been reached. The important point here is that, thanks to the diagonal nature of all the GW quantities (see section 2), their expressions are valid (within the quasiparticle approximation), not only at the zeroth iteration, but at any stage of the self-consistent iterative scheme.

There exists two main types of partially self-consistent GW methods: (i) in *"eigenvalue-only quasiparticle"* GW (evGW),[10,11,36,89] the quasiparticle energies are updated at each iteration; (ii) in *"quasiparticle self-consistent"* GW (qsGW),[57,90−92] one updates both the quasiparticle energies and the corresponding orbitals. Note that a starting point dependency remains in evGW as the orbitals are not self-consistently optimized in that case. However, in the present

DOI: 10.1021/acs.jctc.8b00260
J. Chem. Theory Comput. 2018, 14, 3071−3082

```
procedure SELF-CONSISTENT GW
    Precompute Σ^x, v and Wigner 3j symbols via Eqs. (6), (17) and (12), respectively
    Set ε^{G_{-1}W_{-1}} = ε^{HF} and n = 0
    while max |Δ| < τ do
        Form Δε (Eq. (10)) and Ω (Eq. (14)) using ε^{G_{n-1}W_{n-1}}
        Form Σ^{GW}(ω) following Eq. (16)
        for ℓ = 1, ..., L do
            Solve ω = ε_ℓ^{HF} + Re[Σ_ℓ^{GW}(ω)] to obtain ε_ℓ^{G_nW_n}
        end for
        Δ = ε^{G_nW_n} − ε^{G_{n-1}W_{n-1}}
        n ← n + 1
    end while
    if BSE then
        Compute BSE excitations energies (see Table 1)
    end if
end procedure
```

Figure 2. Pseudocode for self-consistent GW calculations. τ is a user-defined threshold.

model, thanks to the diagonal nature of the various intermediates, the orbitals do not mix from one iteration to another, and the only "updatable" quantities are the quasiparticle energies. Consequently, the partially self-consistent GW schemes evGW and qsGW are strictly equivalent. Hence, we will not be making any distinction between them and label them as GW in the following.

A pseudocode of the self-consistent GW algorithm is reported in Figure 2. In the present implementation, at the nth iteration, the GW quasiparticle orbital energies $\epsilon_I^{G_nW_n}$ are determined by solving the nonlinear, frequency-dependent quasiparticle equation

$$\omega = \epsilon_I^{HF} + Re[\Sigma_I^{GW}(\omega)] \tag{21}$$

Note that Σ^{GW} is built with the orbital energy differences, $\Delta\epsilon$ and RPA excitation energies, Ω computed with the orbital energies from the previous iteration, that is, $\epsilon^{G_{n-1}W_{n-1}}$. The self-consistent process is carried on until the convergence criterion

$$\max |\epsilon^{G_nW_n} - \epsilon^{G_{n-1}W_{n-1}}| < \tau \tag{22}$$

is met (where τ is a user-defined threshold).

The various solutions of the quasiparticle eq 21, $\omega_{I,s}$, have different meanings. For each I value, in addition to the principal quasiparticle energy $\epsilon_{I,0} \equiv \epsilon_I$, there is a finite number of satellites resonances N_I^{sat} at frequencies $\epsilon_{I,s}$ $(s > 0)$ stemming from the poles of the self-energy. One can show that the two sum rules[93]

$$\sum_{s=0}^{N_I^{sat}} Z_I(\epsilon_{I,s}) = 1, \qquad \sum_{s=0}^{N_I^{sat}} Z_I(\epsilon_{I,s})\epsilon_{I,s} = \epsilon_I^{HF} \tag{23}$$

are fulfilled where $Z_I(\omega)$ is given by eq 19.

In a weakly or moderately correlated regime, one can clearly distinguish dominant quasiparticle peaks from satellites, whereas this scenario can break down in the strongly correlated regime. However, as we shall see below, this is not always the case. In the present quasiparticle GW scheme, one only updates the quasiparticle energies, and the satellite resonances are discarded. Hence, the quasiparticle weights are reset to one at each iteration.

3.3. GF2. Diagrammatically, the difference between GW and GF2 is simple to explain: while GW takes into account all the direct ring diagrams, GF2 only includes the two (direct and exchange) second-order diagrams.[6,94,95] Therefore, GF2 does not take into account the screening of the Coulomb interaction. This is illustrated in Figure 3 in terms of Feynman diagrams. Note that GF2 is also known as the second Born approximation.[96] Like in GW, the correlation part of the GF2 self-energy has a diagonal representation

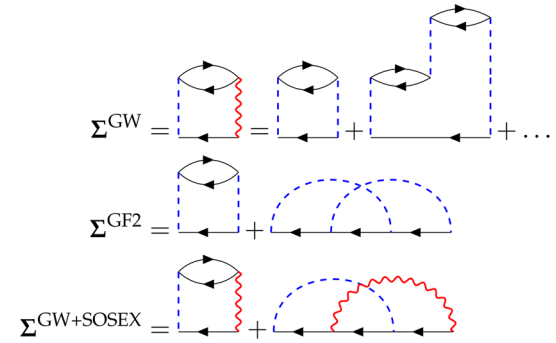

Figure 3. Diagrammatic representation of the correlation part of the GW, GF2, and GW+SOSEX self-energies. Arrowed solid black lines, dashed blue lines, and wiggly red lines indicate the one-body Green function G, the bare Coulomb interaction v, and dynamically screened Coulomb interaction W, respectively. In perturbative or self-consistent calculations, the propagator G is bared or dressed, respectively.

$$\Sigma_I^{GF2}(\omega) = \frac{(1-\delta_{0I})(0II)^2}{\omega - \epsilon_0 + \Delta\epsilon_I - i\eta} + \sum_{I_1,I_2=1}^{L} \frac{2(I_1I_2I)^2 - (I_1I_2I)(I_2I_1I)}{\omega - \epsilon_{I_1} - \Delta\epsilon_{I_2} + i\eta} \tag{24}$$

Similarly to G_0W_0, we consider a one-shot, perturbative GF2 procedure. For sake of consistency, we will label these calculations as G_0F2. The G_0F2 quasiparticle orbital energies $\epsilon_I^{G_0F2}$ are given by eq 18 where one replaces Σ_I^{GW} by Σ_I^{GF2}, with a similar substitution for the renormalization factor reported in eq 19. We also consider a self-consistent version. The self-consistent procedure for GF2 is similar to the self-consistent GW scheme detailed in Figure 2, except that one substitutes the GW self-energy (16) by its GF2 counterpart given by eq 24. From here on, we will label these self-consistent calculations as GF2.

3.4. GW+SOSEX. To combine the best of both worlds, we propose to study a combination of GW and GF2, which is equivalent to the GW+SOSEX method recently introduced by Ren et al.[97] GW+SOSEX is a well-defined diagrammatic

DOI: 10.1021/acs.jctc.8b00260
J. Chem. Theory Comput. 2018, 14, 3071−3082

Table 1. Expression of the lth Singlet Excitation Energy ${}^1\Omega_l$ and the lth Triplet Excitation Energy ${}^3\Omega_l$ for Various Methods[a]

method	singlet excitation energies ${}^1\Omega_l$	triplet excitation energies ${}^3\Omega_l$
CIS	$\Delta\epsilon_l^{\mathrm{HF}} - 2\Sigma_l^{\mathrm{x}} + \Sigma_0^{\mathrm{x}}$	$\Delta\epsilon_l^{\mathrm{HF}} + \Sigma_0^{\mathrm{x}}$
TDHF	$\sqrt{(\Delta\epsilon_l^{\mathrm{HF}} - \Sigma_l^{\mathrm{x}} + \Sigma_0^{\mathrm{x}})(\Delta\epsilon_l^{\mathrm{HF}} - 3\Sigma_l^{\mathrm{x}} + \Sigma_0^{\mathrm{x}})}$	$\sqrt{(\Delta\epsilon_l^{\mathrm{HF}} - \Sigma_l^{\mathrm{x}} + \Sigma_0^{\mathrm{x}})(\Delta\epsilon_l^{\mathrm{HF}} + \Sigma_l^{\mathrm{x}} + \Sigma_0^{\mathrm{x}})}$
RPA	$\sqrt{\Delta\epsilon_l(\Delta\epsilon_l - 4\Sigma_l^{\mathrm{x}})}$	$\Delta\epsilon_l$
BSE	$\sqrt{\left(\Delta\epsilon_l - \Sigma_l^{\mathrm{x}} + \Sigma_0^{\mathrm{x}} - \frac{4(\Sigma_l^{\mathrm{x}})^2}{\Delta\epsilon_l - 4\Sigma_l^{\mathrm{x}}}\right)\left(\Delta\epsilon_l - 3\Sigma_l^{\mathrm{x}} + \Sigma_0^{\mathrm{x}} + \frac{4(\Sigma_l^{\mathrm{x}})^2}{\Delta\epsilon_l - 4\Sigma_l^{\mathrm{x}}}\right)}$	$\sqrt{\left(\Delta\epsilon_l - \Sigma_l^{\mathrm{x}} + \Sigma_0^{\mathrm{x}} - \frac{4(\Sigma_l^{\mathrm{x}})^2}{\Delta\epsilon_l}\right)\left(\Delta\epsilon_l + \Sigma_l^{\mathrm{x}} + \Sigma_0^{\mathrm{x}} + \frac{4(\Sigma_l^{\mathrm{x}})^2}{\Delta\epsilon_l}\right)}$

[a]The lowest excitation corresponds to $l = 1$.

method which adds, like in the SOSEX version of RPA, a subset of higher-order exchange-type diagrams to the formally infinite number of direct ring diagrams from GW (see Figure 3).[98] Unlike Ren et al.,[97] we test both the one-shot version, labeled G_0W_0+SOSEX, as well as its self-consistent version GW +SOSEX. The correlation part of the GW+SOSEX self-energy is given by

$$\Sigma_l^{\mathrm{GW+SOSEX}}(\omega) = \frac{(1-\delta_{0l})[0l|l]^2}{\omega - \epsilon_0 + \Omega_l - i\eta} + \sum_{l_1 l_2=1}^{L} \frac{2[l_1 l_2|l]^2 - [l_1 l_2|l][l_2 l_1|l]}{\omega - \epsilon_{l_1} - \Omega_{l_2} + i\eta} \tag{25}$$

which corresponds to the GF2 expression 24, where one has substituted the bare two-electron integrals (eq 15a) by their screened version (eq 15b) stemming from the GW self-energy expression 16. As we shall see later on, the main advantage of this hybrid method is to partially remove self-screening which hampers the accuracy of the GW method, in particular for few-electron systems.[99−101] Again, the implementation of GW +SOSEX follows closely the algorithm detailed in Figure 2, except that one replaces the GW self-energy (eq 16) by its SOSEX-corrected version given by eq 25.

3.5. Bethe−Salpeter Equation. From the first-order variation of G with respect to a general nonlocal external potential, one can get the neutral excitations of the system. This corresponds to solving the Bethe−Salpeter equation (BSE).[102] Here, we use the BSE within the GW approximation (BSE@GW)[4,103] to study the singlet and triplet neutral excitations of spherium. Note that the BSE calculations are performed as a post-GW step (see Figure 2). We compare BSE with two common quantum chemistry methods: configuration interaction singles (CIS) and time-dependent HF (TDHF). We refer the interested readers to the review of Dreuw and Head-Gordon for more details about these conventional methods.[104]

Thanks to the unique feature of the present model, the linear response eigenvalue problem has a diagonal structure. It implies that the eigenvalues and eigenvectors can be trivially obtained, and the singlet and triplet excitation energies can be easily written in closed form for all the methods mentioned above. Their expressions are gathered in Table 1.

To compute the BSE excitation energies for the singlet and triplet manifolds, one must solve the following linear response problem[105]

$$\begin{pmatrix} \boldsymbol{A} & \boldsymbol{B} \\ \boldsymbol{B} & \boldsymbol{A} \end{pmatrix}\begin{pmatrix} \boldsymbol{X} \\ \boldsymbol{Y} \end{pmatrix} = \Omega \begin{pmatrix} 1 & 0 \\ 0 & -1 \end{pmatrix}\begin{pmatrix} \boldsymbol{X} \\ \boldsymbol{Y} \end{pmatrix} \tag{26}$$

which is usually transformed (when the orbitals do not exhibit triplet instabilities[105]) into an eigenvalue problem of smaller dimension

$$(\boldsymbol{A}-\boldsymbol{B})^{1/2}(\boldsymbol{A}+\boldsymbol{B})(\boldsymbol{A}-\boldsymbol{B})^{1/2}\boldsymbol{Z} = \Omega^2\boldsymbol{Z} \tag{27}$$

where the excitation amplitudes are

$$\boldsymbol{X}+\boldsymbol{Y} = \Omega^{-1/2}(\boldsymbol{A}-\boldsymbol{B})^{1/2}\boldsymbol{Z} \tag{28}$$

The only difference between CIS, TDHF, RPA, and BSE lies in the specific expression of the matrix elements of $\boldsymbol{A}$ and $\boldsymbol{B}$. As mentioned above, in the present case, the matrices $\boldsymbol{A}$ and $\boldsymbol{B}$ have a diagonal structure, and the BSE diagonal elements are given by

$$A_l^{\mathrm{BSE}} = A_l^{\mathrm{RPA}} + \delta A_l^{\mathrm{BSE}}, \quad B_l^{\mathrm{BSE}} = B_l^{\mathrm{RPA}} + \delta B_l^{\mathrm{BSE}} \tag{29}$$

where the RPA part is

$$A_l^{\mathrm{RPA}} = \Delta\epsilon_l - 2(1-\delta_{\sigma\sigma'})\Sigma_l^{\mathrm{x}}, \quad B_l^{\mathrm{RPA}} = -2(1-\delta_{\sigma\sigma'})\Sigma_l^{\mathrm{x}} \tag{30}$$

and the BSE correction reads

$$\delta A_l^{\mathrm{BSE}} = \Sigma_0^{\mathrm{x}}, \quad \delta B_l^{\mathrm{BSE}} = \Sigma_l^{\mathrm{x}} - \frac{4(\Sigma_l^{\mathrm{x}})^2}{A_l^{\mathrm{RPA}} + B_l^{\mathrm{RPA}}} \tag{31}$$

with

$$\delta_{\sigma\sigma'} = \begin{cases} 0, & \sigma \neq \sigma' \text{ (singlet manifold)} \\ 1, & \sigma = \sigma' \text{ (triplet manifold)} \end{cases} \tag{32}$$

Therefore, substituting eq 30 into eq 27 yields the BSE excitation energy

$$\Omega_l^{\mathrm{BSE}} = \sqrt{(A_l^{\mathrm{BSE}} - B_l^{\mathrm{BSE}})(A_l^{\mathrm{BSE}} + B_l^{\mathrm{BSE}})} \tag{33}$$

Their explicit expression for the singlet and triplet manifold are provided in Table 1. The CIS, TDHF, and RPA excitations energies can be obtained via the same derivation and their expressions are also reported in Table 1.

3.6. Correlation Energy. The correlation energy is defined as

$$E_{\mathrm{c}} = E - E_{\mathrm{HF}} \tag{34}$$

where E is a total energy estimate provided by a given correlated method and $E_{\mathrm{HF}} = 1/R$ is the (restricted) HF energy of the singlet ground-state of spherium.[75]

We followed two distinct routes to estimate the correlation energy within GW. First, we estimated the correlation energy within the RPA[15,106−108]

DOI: 10.1021/acs.jctc.8b00260
J. Chem. Theory Comput. 2018, 14, 3071−3082

$$E_c^{\mathrm{RPA}} = -\sum_{I=1}^{L} (A_I^{\mathrm{RPA}} - \Omega_I) \tag{35}$$

where the A_I^{RPA} and Ω_I values are given by eqs 30 and 14, respectively. We note that eq 35 can be obtained from the variational Klein functional[109] if the GW approximation is used for the Luttinger−Ward (or Φ) functional.[110]

The second route we followed was to calculate the functional[34,46]

$$E_c^{\mathrm{GM}} = \frac{-i}{2}\sum_{I=0}^{\infty}\int \frac{d\omega}{2\pi}\Sigma_I^c(\omega)G_I(\omega)e^{i\omega\eta} \tag{36}$$

This equation is equivalent to the correlation part of the Galitskii−Migdal (GM) functional[111] for the total energy if the self-energy and the Green function are connected through the Dyson equation. For this reasons, we will refer to the above expression as the GM functional for the correlation energy. In our case, the frequency integration in eq 36 can be performed analytically. We obtain

$$E_c^{\mathrm{GM@GW}} = -2\sum_{I=1}^{L} \frac{[0II]^2 + [II0]^2}{\Delta\epsilon_I + \Omega_I} \tag{37a}$$

$$E_c^{\mathrm{GM@GF2}} = -\sum_{I=1}^{L} \frac{(0II)^2 + (II0)^2}{\Delta\epsilon_I + \Delta\epsilon_I} \tag{37b}$$

$$E_c^{\mathrm{GM@GW+SOSEX}} = -\sum_{I=1}^{L} \frac{[0II]^2 + [II0]^2}{\Delta\epsilon_I + \Omega_I} \tag{37c}$$

where the denominator of eq 37b has been written in such a way to highlight its similarity with eqs 37a and 37c.

As evidenced by eqs 37a and 37c, we have $E_c^{\mathrm{GM@GW+SOSEX}} = \frac{1}{2}E_c^{\mathrm{GM@GW}}$. As discussed in the next section this is related to the self-screening problem of GW. Note that the correlation energy provided by the RPA and the GM functional within the GW approximation are equal only at full self-consistency.[32−34] Since we only consider partially self-consistent GW schemes here, the two energy estimates will differ.[41]

For comparison purposes, we have also computed the second-order Møller−Plesset (MP2) correlation energy,[112] which reads

$$E_c^{\mathrm{MP2}} = -\sum_{I=1}^{L} \frac{(0II)^2}{\Delta\epsilon_I + \Delta\epsilon_I} \tag{38}$$

It is interesting to note the similarity between the MP2 expression (eq 38) and the GM expressions reported in eqs 37a, 37b, and 37c.

4. RESULTS

4.1. Computational Details. In practice, one only requires the energy of the main quasiparticle peaks at each iteration (i.e., the satellites can be discarded). For each I value, the quasiparticle energy is found by solving the quasiparticle equation (see, for example, eq 21) using Newton's method (as implemented in Mathematica 11) starting from the result of the previous iteration. To avoid finite-size basis set effects, the maximum angular momentum of the basis set has been set to $L = 50$, which ensures converged results with respect to the basis set size up to $R = 10$, the largest radius considered here. However, we only update the eigenvalues for $0 \leq I \leq 10$, which corresponds to the HOMO ($I = 0$), the LUMO ($I = 1$), and the next nine unoccupied orbitals. As mentioned earlier, all the calculations have been performed with a (restricted) HF starting point.[75] For the self-consistent GW calculations, the convergence threshold has been set to $\tau = 10^{-5}$. In case of convergence issues, instead of the usual linear mixing performed in standard implementations,[29,33] we have found that the DIIS extrapolation technique originally proposed by Pulay[113,114] is more robust and rather efficient.

The quantities labeled as "exact" have been obtained from near-exact calculations computed with the full configuration interaction (FCI) method.[75] In particular, to obtain the exact ionization potential, electron affinity and gap of the two-electron system, we have computed the exact ground-state total energies of the one-, two-, and three-electron systems for various R values, as well as the singlet and triplet excitation energies of the two-electron system. For some well-defined values of R (such as $R = \sqrt{3}/2$ or $\sqrt{7}$), exact wave functions and energies are available in the case of the two-electron system.[76,84] Finally, we note that we have verified that the sum rules in eq 23 are satisfied in our calculations.

4.2. Ionization Potential, Electron Affinity, and Energy Gap. The ionization potential (IP) and electron affinity (EA) are defined as[112]

$$\mathrm{IP} = -\epsilon_{\mathrm{HOMO}}, \qquad \mathrm{EA} = -\epsilon_{\mathrm{LUMO}} \tag{39}$$

where ϵ_{HOMO} and ϵ_{LUMO} are the HOMO ($I = 0$) and LUMO ($I = 1$) orbital energies, respectively, while the energy gap is

$$E_{\mathrm{gap}} = \epsilon_{\mathrm{LUMO}} - \epsilon_{\mathrm{HOMO}} = \mathrm{IP} - \mathrm{EA} \tag{40}$$

These results are shown in Figure 4, where we have reported the relative error (in %) on IP, EA, and E_{gap} as a function of R for various methods from the weakly correlated regime ($R \ll 1$) to the strongly correlated regime ($R \gg 1$). (The associated numerical results can be found in Tables I−III in the Supporting Information.)

The first striking observation is the quality of G_0F2 (solid blue curve in Figure 4), which yields accurate results up to $R \approx 2$, a regime in which the system can certainly be considered as weakly correlated. Indeed, for two-electron systems, GF2 is known to be particularly accurate.[115−117] However, within GF2 and GW, the effect of self-consistency is disappointing. For example, the perturbative G_0W_0 version (solid red curve) yields more accurate estimates than its self-consistent counterpart (dashed red curve). Similar observations can be made for GF2 (blue lines) although the self-consistency starts deteriorating the results at larger R.

G_0W_0 and GW are particularly bad at reproducing the ionization energies, even in the high-density (i.e., small-R) limit. The electron affinities are better reproduced, while E_{gap} benefits from error cancellations (at least for small R). This indicates that the poor performance of GW for the IP is mainly due to self-screening, that is, the hole that is left behind after ionization is not just screened by the electron that remains but also by the electron that is removed.[73,99,101,118] This is clearly not physical and happens only for the IP; for the EA, the additional electron is correctly screened by both electrons.

Indeed, GW+SOSEX (dashed green line), which is mostly self-screening-free, does a decent job for the IP, although it still overestimates at large R. The SOSEX correction significantly improves the EA, but E_{gap} is slightly less accurate for

DOI: 10.1021/acs.jctc.8b00260
J. Chem. Theory Comput. 2018, 14, 3071−3082

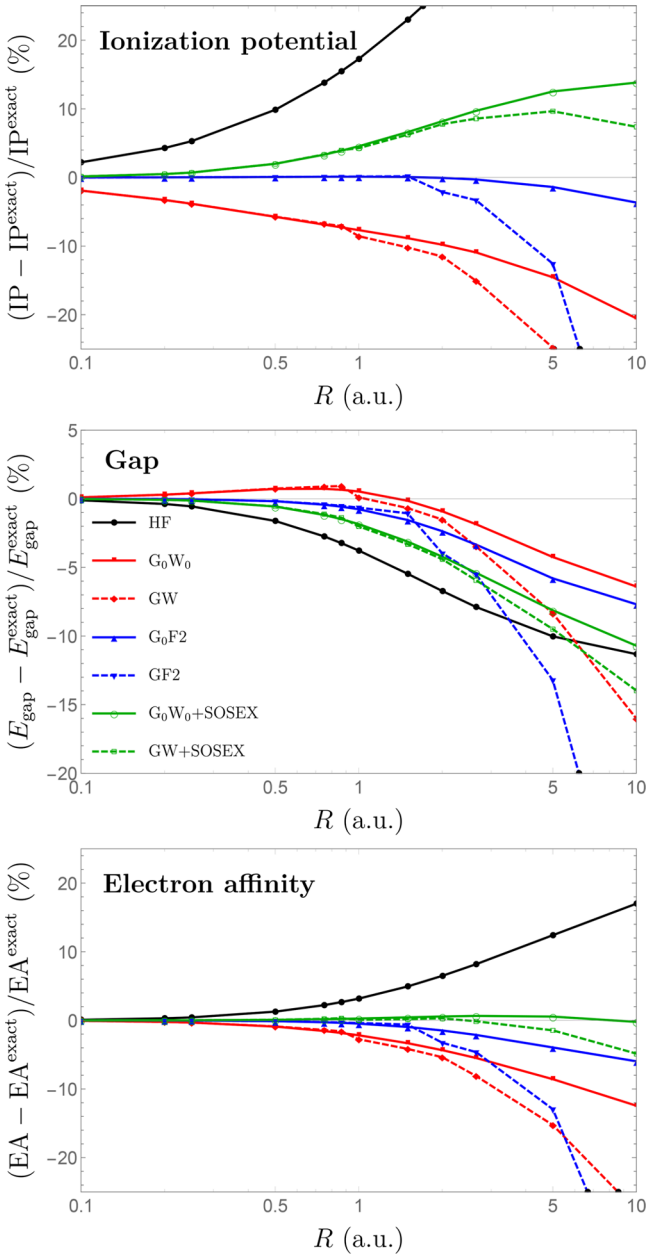

Figure 4. Relative error (in %) on IP (top), E_{gap} (middle), and EA (bottom) as a function of R for various schemes. See the Supporting Information for raw data.

intermediate R values. This behavior is consistent with the findings of Knight et al.[66] In the case of GW+SOSEX, the effect of self-consistency is also disappointing and, except for the IP, deteriorates the results compared to the perturbative version.

Finally, we note that discontinuities appear around $R = 1$ and 2 in the case of GW and GF2, respectively. We will discuss this in more detail in section 4.5.

4.3. Neutral Excitations. Figure 5 shows the relative error (in %) for the lowest singlet (left) and triplet (right) excitation energies (i.e., $l = 1$) as a function of R for various methods. (The associated numerical results can be found in Tables IV and V in the Supporting Information.) Because for $R > 3/2$ triplet instabilities appear due to the existence of a lower-energy (symmetry-broken) HF solution,[75] we restrict our study to the high-density region $0 < R \leq 3/2$.

Because the GW eigenvalues are not significantly modified by the level of self-consistency in the high-density region (as one can see from Figure 4), we have chosen not to report the G_0W_0 curves which are very similar (yet not strictly identical) to the self-consistent GW ones depicted in Figure 5. In other words, the BSE excitations do not depend strongly on the input GW eigenvalues.

Concerning the singlet manifold (left graph of Figure 5), TDHF is the most reliable method. Although BSE@GW appears as the least accurate method, it yields singlet excitation energies within a few percents of the FCI results. BSE@GW +SOSEX shows significant improvement compared to the SOSEX-free methods. Again, one can notice the discontinuity around $R = 1$ in the BSE@GW curve (see below).

For the triplet manifold (right graph of Figure 5), BSE@GW outperforms more conventional methods, such as CIS and TDHF as well as BSE@GW+SOSEX and BSE@GF2. Note, however, that the magnitude of the errors for the triplet excitations are much larger than for the singlet ones. This behavior is also observed in molecular systems[58] because of the inadequate singlet reference wave function used in most cases.[105]

4.4. Correlation Energy. Concerning the correlation energy of spherium, the results are represented in Figure 6. (The associated numerical results can be found in Table VI in the Supporting Information.)

MP2 (see eq 38) provides a fairly consistent and reliable estimate of the correlation energy in the weakly correlated regime, although the relative error increases slightly when one gets to the strongly correlated regime where Møller−Plesset perturbation theory naturally breaks down.[112]

First, let us mention that, in the weakly correlated regime, as expected, the correlation energies obtained with perturbative and self-consistent methods are very similar. This has also been observed for atoms and molecules.[41,42,107,119−123] However, the situation is different in the strongly correlated regime and, for $R > 2$, the perturbative and its self-consistent variant start to deviate.

Because of its relation to the variational Klein functional, E_c^{RPA} is also independent of the approximation to the self-energy up to $R \approx 2$. Interestingly, even in the large-R regime, the RPA yields decent E_c estimates with a maximum error of ∼20%.

Unlike E_c^{RPA}, the GM functional (known to be nonvariational) is strongly dependent on the quality of G, and generally yields too negative correlation energies, an observation already made by several authors for the uniform electron gas,[47−49] solids,[53,54] atoms and molecules.[32−34,41] The self-screening in GW has a huge effect on E_c^{GM}. For example, GM@GW is consistently wrong by about a factor two. When one improves the Green function, for instance by the introduction of second-order exchange, E_c^{GM} gets closer to the values obtained with E_c^{RPA}. In particular, GM@SOSEX, which removes most of the self-screening in GW, greatly improves the correlation energy, and even becomes more accurate than MP2 at large R.

For the correlation energies the influence of self-consistency is ambiguous. While self-consistency improves the correlation energies in the case of E_c^{RPA}, they deteriorate for E_c^{GM}.

4.5. Binary System. As mentioned several times earlier in this manuscript, there is an obvious discontinuity in Figures 4−6) around $R \approx 0.9$. Note that this "glitch" is only present in self-consistent calculations and is more pronounced in the SOSEX-free GW version. Note also that its magnitude is small

DOI: 10.1021/acs.jctc.8b00260
J. Chem. Theory Comput. 2018, 14, 3071−3082

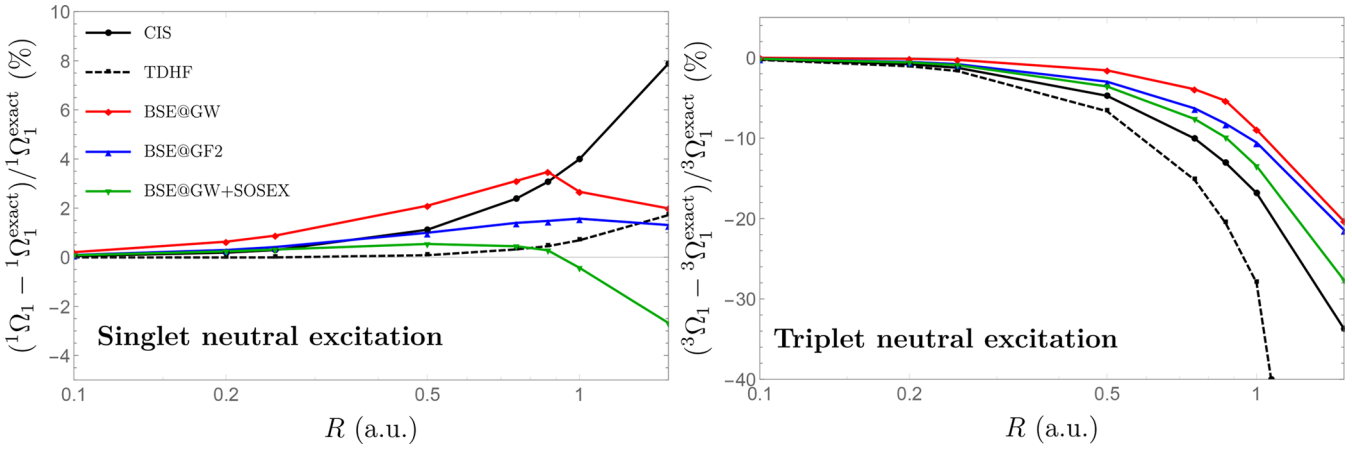

Figure 5. Relative error (in %) on the lowest singlet excitation $^1\Omega_1$ (left) and the lowest triplet excitation $^3\Omega_1$ (right) as a function of R for various schemes. Note the different scales of the two graphs. See the Supporting Information for raw data.

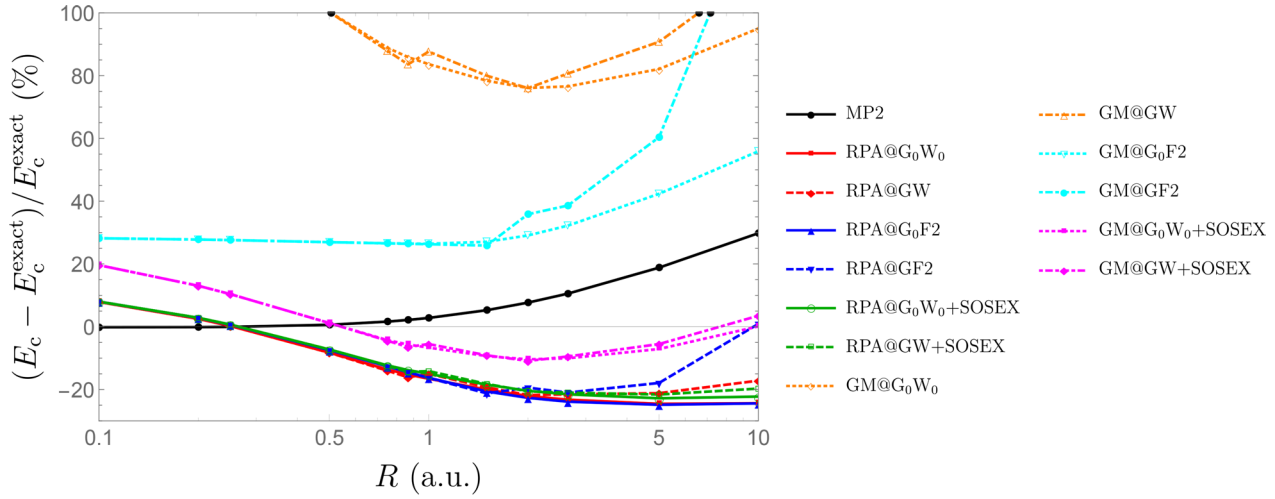

Figure 6. Relative error (in %) on the correlation energy E_c as a function of R for various schemes. See the Supporting Information for raw data.

(yet numerically significant) and one would hardly notice it by looking at absolute energies. From a technical point of view, the left and right sides of the discontinuity originate from two distinct solutions of the quasiparticle equation. We note that this problem is different from the unphysical solutions discussed in ref 72.

Our analysis has shown that this discontinuity is caused by the proximity of the quasiparticle peak of the LUMO+1 orbital (at $\epsilon_2 \equiv \epsilon_{2,0} \approx 4.3$) and a singularity of Σ_2^{GW} (at $\epsilon_1 + \Omega_1 \approx 4.8$). This is illustrated in Figure 7 for a sphere of unit radius. Because of the local symmetry of Σ^{GW} at the vicinity of a singularity, it implies the existence of a satellite resonance (at $\epsilon_{2,1} \approx 5.2$) having a weight $Z_2(\epsilon_{2,1})$ of similar magnitude as the main quasiparticle peak $Z_2(\epsilon_{2,0})$. In that case, one cannot really talk about a quasiparticle peak and its satellite. It would be more appropriate to describe this peculiar situation as a binary system where both resonances have similar weights. Figure 7 clearly shows the presence of two large-weight peaks for the LUMO+1 (thick cyan curve). For these two peaks, we have reported, in the inset graph of Figure 7, $Z_l(\epsilon_{l,s})$ as a function of R. We see that, outside the range $1/2 \leq R \leq 3/2$, one resonance prevails over the other. However, for $R \approx 1$ the weight of the two resonances become similar and they cross around $R \approx 0.85$. Therefore, depending on the value of R, the self-consistent process selects one or the other solution depending on their relative weights. This ultimately leads to a discontinuity in the self-consistent result for the quasiparticle energies.

Although a similar issue has been observed in G_0W_0 by van Setten and co-workers,[22,63] to be best of our knowledge, this type of observation has never been reported in the literature for self-consistent GW schemes. Note that all this happens in the weakly correlated regime, where one should safely assume the validity of the quasiparticle picture. We believe that such discontinuity would not exist within a fully self-consistent scheme where one takes into account the quasiparticle peak, as well as its satellites at each iteration. If confirmed, this would be a strong argument in favor of fully self-consistent schemes. Finally, we note that these discontinuities are ubiquitous: they also appear for higher-energy orbitals and for larger radii. We are currently analyzing the cause of such discontinuities in more details.

5. CONCLUSION

We have provided an exhaustive study of the performance of different commonly used variants of Green function methods for the two-electron spherium model. We found that, in general, self-consistency deteriorates the results with respect to those obtained within perturbative GW starting from Hartree–

DOI: 10.1021/acs.jctc.8b00260
J. Chem. Theory Comput. 2018, 14, 3071−3082

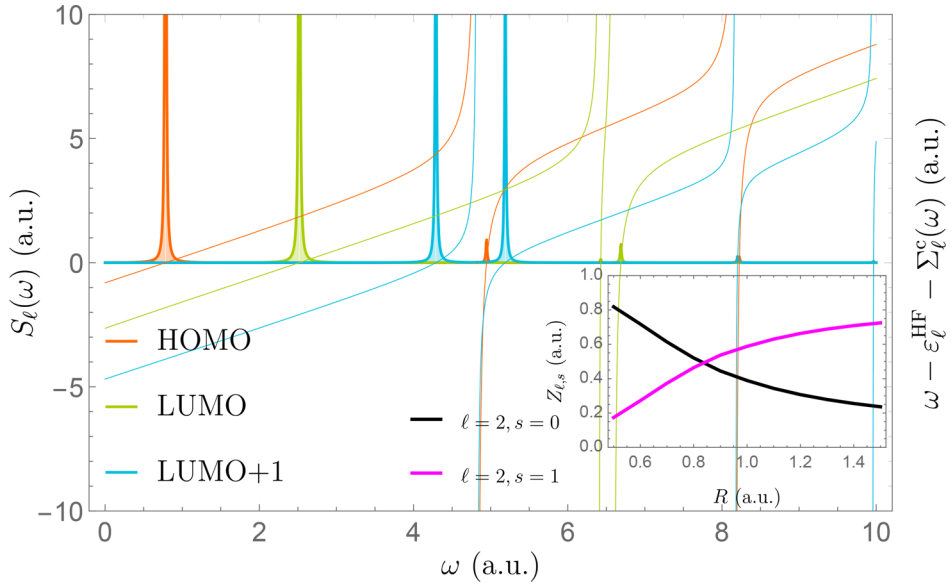

Figure 7. Self-consistent GW spectral function $S_l(\omega)$ as a function of ω (thick lines) for the HOMO (orange), LUMO (green), and LUMO+1 (cyan) orbitals at $R = 1$ and for $\eta = 10^{-3}$. The solutions of the quasiparticle equation are located at the intersection of the thin curves $\omega - \epsilon_l^{HF} - Re[\Sigma_l^{GW}(\omega)]$ and the horizontal axis. The inset graph reports the renormalization factor $Z_l(\epsilon_{l,s})$ of the LUMO+1 (i.e., $l = 2$) for the quasparticle peak ($s = 0$, black curve) and the first satellite ($s = 1$, magenta curve) as a function of R.

Fock orbital energies. This is the case for many properties of interest, such as ionization potentials, electron affinities, and energy gaps. Only for RPA correlation energies do we observe a small improvement when doing the calculations self-consistently. We showed that the same is true for GF2, that is, self-consistent GF2 results are, in general, worse than those obtained perturbatively. We have also discussed the problem of self-screening in GW and showed that it can be partially cured by adding a second-order screened exchange (SOSEX) correction. We observe that this correction generally improves results. However, here again, self-consistency is disappointing. Finally, we have evidenced that partially self-consistent GW can lead to artificial discontinuities in the self-energy. We traced this problem back to the appearance of a satellite resonance with a weight similar to that of the quasiparticle.

■ ASSOCIATED CONTENT

Supporting Information

The Supporting Information is available free of charge on the ACS Publications website at DOI: 10.1021/acs.jctc.8b00260.

Raw data for Figures 4–6 (PDF)

■ AUTHOR INFORMATION

Corresponding Author

*E-mail: loos@irsamc.ups-tlse.fr.

ORCID

Pierre-François Loos: 0000-0003-0598-7425

Notes

The authors declare no competing financial interest.

■ ACKNOWLEDGMENTS

The authors would like to thank Fabio Caruso, Fabien Bruneval, Denis Jacquemin, and Xavier Blase for helpful discussions about GW methods.

■ REFERENCES

(1) Aryasetiawan, F.; Gunnarsson, O. The GW method. *Rep. Prog. Phys.* **1998**, *61*, 237–312.

(2) Onida, G.; Reining, L.; Rubio, A. Electronic excitations: density-functional versus many-body Green's-function approaches. *Rev. Mod. Phys.* **2002**, *74*, 601.

(3) Reining, L. The GW Approximation: Content, Successes and Limitations: The GW Approximation. *Wiley Interdiscip. Rev. Comput. Mol. Sci.* **2018**, *8*, No. e1344.

(4) Blase, X.; Duchemin, I.; Jacquemin, D. The Bethe–Salpeter Equation in Chemistry: Relations with TD-DFT, Applications and Challenges. *Chem. Soc. Rev.* **2018**, *47*, 1022–1043.

(5) Danovich, D. Green's Function Methods for Calculating Ionization Potentials, Electron Affinities, and Excitation Energies: GF Methods for Calculating IPs, EAs, and Excitation Energies. *Wiley Interdiscip. Rev. Comput. Mol. Sci.* **2011**, *1*, 377–387.

(6) Ortiz, J. V. Electron Propagator Theory: An Approach to Prediction and Interpretation in Quantum Chemistry: Electron Propagator Theory. *Wiley Interdiscip. Rev. Comput. Mol. Sci.* **2013**, *3*, 123–142.

(7) Fetter, A. L.; Waleck, J. D. *Quantum Theory of Many Particle Systems*; McGraw Hill: San Francisco, 1971.

(8) Hedin, L. New Method for Calculating the One-Particle Green's Function with Application to the Electron-Gas Problem. *Phys. Rev.* **1965**, *139*, A796.

(9) Olver, F. W. J., Lozier, D. W., Boisvert, R. F., Clark, C. W., Eds. *NIST Handbook of Mathematical Functions*; Cambridge University Press: New York, 2010.

(10) Blase, X.; Attaccalite, C.; Olevano, V. First-Principles GW Calculations for Fullerenes, Porphyrins, Phtalocyanine, and Other Molecules of Interest for Organic Photovoltaic Applications. *Phys. Rev. B: Condens. Matter Mater. Phys.* **2011**, *83*, 115103.

(11) Faber, C.; Attaccalite, C.; Olevano, V.; Runge, E.; Blase, X. First-Principles GW Calculations for DNA and RNA Nucleobases. *Phys. Rev. B: Condens. Matter Mater. Phys.* **2011**, *83*, 115123.

(12) Bruneval, F. Ionization Energy of Atoms Obtained from *GW* Self-Energy or from Random Phase Approximation Total Energies. *J. Chem. Phys.* **2012**, *136*, 194107.

DOI: 10.1021/acs.jctc.8b00260
J. Chem. Theory Comput. 2018, 14, 3071–3082

(13) Bruneval, F.; Marques, M. A. L. Benchmarking the Starting Points of the *GW* Approximation for Molecules. *J. Chem. Theory Comput.* **2013**, *9*, 324−329.
(14) Bruneval, F.; Hamed, S. M.; Neaton, J. B. A Systematic Benchmark of the *Ab Initio* Bethe-Salpeter Equation Approach for Low-Lying Optical Excitations of Small Organic Molecules. *J. Chem. Phys.* **2015**, *142*, 244101.
(15) Bruneval, F.; Rangel, T.; Hamed, S. M.; Shao, M.; Yang, C.; Neaton, J. B. Molgw 1: Many-Body Perturbation Theory Software for Atoms, Molecules, and Clusters. *Comput. Phys. Commun.* **2016**, *208*, 149−161.
(16) Bruneval, F. Optimized Virtual Orbital Subspace for Faster GW Calculations in Localized Basis. *J. Chem. Phys.* **2016**, *145*, 234110.
(17) Boulanger, P.; Jacquemin, D.; Duchemin, I.; Blase, X. Fast and Accurate Electronic Excitations in Cyanines with the Many-Body Bethe−Salpeter Approach. *J. Chem. Theory Comput.* **2014**, *10*, 1212−1218.
(18) Blase, X.; Boulanger, P.; Bruneval, F.; Fernandez-Serra, M.; Duchemin, I. *GW* and Bethe-Salpeter Study of Small Water Clusters. *J. Chem. Phys.* **2016**, *144*, 034109.
(19) Li, J.; Holzmann, M.; Duchemin, I.; Blase, X.; Olevano, V. Helium Atom Excitations by the G W and Bethe-Salpeter Many-Body Formalism. *Phys. Rev. Lett.* **2017**, *118*, 163001.
(20) Hung, L.; da Jornada, F. H.; Souto-Casares, J.; Chelikowsky, J. R.; Louie, S. G.; Öğüt, S. Excitation Spectra of Aromatic Molecules within a Real-Space G W -BSE Formalism: Role of Self-Consistency and Vertex Corrections. *Phys. Rev. B: Condens. Matter Mater. Phys.* **2016**, *94*, 085125.
(21) Hung, L.; Bruneval, F.; Baishya, K.; Öğüt, S. Benchmarking the *GW* Approximation and Bethe−Salpeter Equation for Groups IB and IIB Atoms and Monoxides. *J. Chem. Theory Comput.* **2017**, *13*, 2135−2146.
(22) van Setten, M. J.; Caruso, F.; Sharifzadeh, S.; Ren, X.; Scheffler, M.; Liu, F.; Lischner, J.; Lin, L.; Deslippe, J. R.; Louie, S. G.; Yang, C.; Weigend, F.; Neaton, J. B.; Evers, F.; Rinke, P. *GW* 100: Benchmarking G_0W_0 for Molecular Systems. *J. Chem. Theory Comput.* **2015**, *11*, 5665−5687.
(23) van Setten, M. J.; Costa, R.; Viñes, F.; Illas, F. Assessing *GW* Approaches for Predicting Core Level Binding Energies. *J. Chem. Theory Comput.* **2018**, *14*, 877−883.
(24) Ou, Q.; Subotnik, J. E. Comparison between *GW* and Wave-Function-Based Approaches: Calculating the Ionization Potential and Electron Affinity for 1D Hubbard Chains. *J. Phys. Chem. A* **2016**, *120*, 4514−4525.
(25) Ou, Q.; Subotnik, J. E. Comparison between the Bethe−Salpeter Equation and Configuration Interaction Approaches for Solving a Quantum Chemistry Problem: Calculating the Excitation Energy for Finite 1D Hubbard Chains. *J. Chem. Theory Comput.* **2018**, *14*, 527−542.
(26) Faber, C. Electronic, Excitonic and Polaronic Properties of Organic Systems within the Many-Body GW and Bethe-Salpeter Formalisms: Towards Organic Photovoltaics. PhD Thesis, Université de Grenoble, 2014.
(27) van Setten, M. J.; Weigend, F.; Evers, F. The *GW* -Method for Quantum Chemistry Applications: Theory and Implementation. *J. Chem. Theory Comput.* **2013**, *9*, 232−246.
(28) Kaplan, F.; Weigend, F.; Evers, F.; van Setten, M. J. Off-Diagonal Self-Energy Terms and Partially Self-Consistency in GW Calculations for Single Molecules: Efficient Implementation and Quantitative Effects on Ionization Potentials. *J. Chem. Theory Comput.* **2015**, *11*, 5152−5160.
(29) Kaplan, F.; Harding, M. E.; Seiler, C.; Weigend, F.; Evers, F.; van Setten, M. J. Quasi-Particle Self-Consistent *GW* for Molecules. *J. Chem. Theory Comput.* **2016**, *12*, 2528−2541.
(30) Krause, K.; Klopper, W. Implementation of the Bethe-Salpeter Equation in the TURBOMOLE Program. *J. Comput. Chem.* **2017**, *38*, 383−388.
(31) Caruso, F.; Rinke, P.; Ren, X.; Scheffler, M.; Rubio, A. Unified Description of Ground and Excited States of Finite Systems: The Self-Consistent G W Approach. *Phys. Rev. B: Condens. Matter Mater. Phys.* **2012**, *86*, No. 081102.
(32) Caruso, F.; Rohr, D. R.; Hellgren, M.; Ren, X.; Rinke, P.; Rubio, A.; Scheffler, M. Bond Breaking and Bond Formation: How Electron Correlation Is Captured in Many-Body Perturbation Theory and Density-Functional Theory. *Phys. Rev. Lett.* **2013**, *110*, 146403.
(33) Caruso, F.; Rinke, P.; Ren, X.; Rubio, A.; Scheffler, M. Self-Consistent G W: All-Electron Implementation with Localized Basis Functions. *Phys. Rev. B: Condens. Matter Mater. Phys.* **2013**, *88*, 075105.
(34) Caruso, F. Self-Consistent GW Approach for the Unified Description of Ground and Excited States of Finite Systems. PhD Thesis, Freie Universität Berlin, 2013.
(35) Hybertsen, M. S.; Louie, S. G. First-Principles Theory of Quasiparticles: Calculation of Band Gaps in Semiconductors and Insulators. *Phys. Rev. Lett.* **1985**, *55*, 1418−1421.
(36) Hybertsen, M. S.; Louie, S. G. Electron Correlation in Semiconductors and Insulators: Band Gaps and Quasiparticle Energies. *Phys. Rev. B: Condens. Matter Mater. Phys.* **1986**, *34*, 5390−5413.
(37) Martin, P. C.; Schwinger, J. Theory of Many-Particle Systems. *Phys. Rev.* **1959**, *115*, 1342−1373.
(38) Baym, G.; Kadanoff, L. P. Conservation Laws and Correlation Functions. *Phys. Rev.* **1961**, *124*, 287−299.
(39) Baym, G. Self-Consistent Approximations in Many-Body Systems. *Phys. Rev.* **1962**, *127*, 1391−1401.
(40) Martin, R. M.; Reining, L.; Ceperley, D. *Interacting Electrons: Theory and Computational Approaches*; Cambridge University Press: New York, NY, 2016.
(41) Stan, A.; Dahlen, N. E.; van Leeuwen, R. Fully Self-Consistent *GW* Calculations for Atoms and Molecules. *Europhys. Lett. EPL* **2006**, *76*, 298−304.
(42) Stan, A.; Dahlen, N. E.; van Leeuwen, R. Levels of Self-Consistency in the GW Approximation. *J. Chem. Phys.* **2009**, *130*, 114105.
(43) Rostgaard, C.; Jacobsen, K. W.; Thygesen, K. S. Fully Self-Consistent GW Calculations for Molecules. *Phys. Rev. B: Condens. Matter Mater. Phys.* **2010**, *81*, 085103.
(44) Koval, P.; Foerster, D.; Sánchez-Portal, D. Fully Self-Consistent G W and Quasiparticle Self-Consistent G W for Molecules. *Phys. Rev. B: Condens. Matter Mater. Phys.* **2014**, *89*, 155417.
(45) Wilhelm, J.; Golze, D.; Talirz, L.; Hutter, J.; Pignedoli, C. A. Toward *GW* Calculations on Thousands of Atoms. *J. Phys. Chem. Lett.* **2018**, *9*, 306−312.
(46) Holm, B.; von Barth, U. Fully Self-Consistent GW Self-Energy of the Electron Gas. *Phys. Rev. B: Condens. Matter Mater. Phys.* **1998**, *57*, 2108.
(47) Holm, B. Total Energies from GW Calculations. *Phys. Rev. Lett.* **1999**, *83*, 788−791.
(48) Holm, B.; Aryasetiawan, F. Total Energy from the Galitskii-Migdal Formula Using Realistic Spectral Functions. *Phys. Rev. B: Condens. Matter Mater. Phys.* **2000**, *62*, 4858.
(49) García-González, P.; Godby, R. W. Self-Consistent Calculation of Total Energies of the Electron Gas Using Many-Body Perturbation Theory. *Phys. Rev. B: Condens. Matter Mater. Phys.* **2001**, *63*, 075112.
(50) Loos, P.-F.; Gill, P. M. W. The Uniform Electron Gas: The Uniform Electron Gas. *Wiley Interdiscip. Rev. Comput. Mol. Sci.* **2016**, *6*, 410−429.
(51) Schöne, W.-D.; Eguiluz, A. G. Self-Consistent Calculations of Quasiparticle States in Metals and Semiconductors. *Phys. Rev. Lett.* **1998**, *81*, 1662−1665.
(52) Ku, W.; Eguiluz, A. G. Band-Gap Problem in Semiconductors Revisited: Effects of Core States and Many-Body Self-Consistency. *Phys. Rev. Lett.* **2002**, *89*, 126401.
(53) Kutepov, A. L. Electronic Structure of Na, K, Si, and LiF from Self-Consistent Solution of Hedin's Equations Including Vertex Corrections. *Phys. Rev. B: Condens. Matter Mater. Phys.* **2016**, *94*, 155101.
(54) Kutepov, A. L.; Kotliar, G. One-Electron Spectra and Susceptibilities of the Three-Dimensional Electron Gas from Self-

DOI: 10.1021/acs.jctc.8b00260
J. Chem. Theory Comput. 2018, 14, 3071−3082

Consistent Solutions of Hedin's Equations. *Phys. Rev. B: Condens. Matter Mater. Phys.* **2017**, *96*, 035108.
(55) de Groot, H. J.; Bobbert, P. A.; van Haeringen, W. Self-Consistent *GW* for a Quasi-One-Dimensional Semiconductor. *Phys. Rev. B: Condens. Matter Mater. Phys.* **1995**, *52*, 11000−11007.
(56) Friedrich, C.; Schindlmayr, A.; Blügel, S.; Kotani, T. Elimination of the Linearization Error in *GW* Calculations Based on the Linearized Augmented-Plane-Wave Method. *Phys. Rev. B: Condens. Matter Mater. Phys.* **2006**, *74*, 045104.
(57) Ke, S.-H. All-Electron G W Methods Implemented in Molecular Orbital Space: Ionization Energy and Electron Affinity of Conjugated Molecules. *Phys. Rev. B: Condens. Matter Mater. Phys.* **2011**, *84*, 205415.
(58) Jacquemin, D.; Duchemin, I.; Blondel, A.; Blase, X. Benchmark of Bethe-Salpeter for Triplet Excited-States. *J. Chem. Theory Comput.* **2017**, *13*, 767−783.
(59) Curtiss, L. A.; Raghavachari, K.; Trucks, G. W.; Pople, J. A. Gaussian-2 Theory for Molecular Energies of First- and Second-row Compounds. *J. Chem. Phys.* **1991**, *94*, 7221−7230.
(60) Schreiber, M.; Silva-Junior, M. R.; Sauer, S. P. A.; Thiel, W. Benchmarks for Electronically Excited States: CASPT2, CC2, CCSD, and CC3. *J. Chem. Phys.* **2008**, *128*, 134110.
(61) Silva-Junior, M. R.; Schreiber, M.; Sauer, S. P. A.; Thiel, W. Benchmarks of Electronically Excited States: Basis Set Effects on CASPT2 Results. *J. Chem. Phys.* **2010**, *133*, 174318.
(62) Silva-Junior, M. R.; Sauer, S. P.; Schreiber, M.; Thiel, W. Basis Set Effects on Coupled Cluster Benchmarks of Electronically Excited States: CC3, CCSDR(3) and CC2. *Mol. Phys.* **2010**, *108*, 453−465.
(63) Maggio, E.; Liu, P.; van Setten, M. J.; Kresse, G. *GW* 100: A Plane Wave Perspective for Small Molecules. *J. Chem. Theory Comput.* **2017**, *13*, 635−648.
(64) Richard, R. M.; Marshall, M. S.; Dolgounitcheva, O.; Ortiz, J. V.; Brédas, J.-L.; Marom, N.; Sherrill, C. D. Accurate Ionization Potentials and Electron Affinities of Acceptor Molecules I. Reference Data at the CCSD(T) Complete Basis Set Limit. *J. Chem. Theory Comput.* **2016**, *12*, 595−604.
(65) Gallandi, L.; Marom, N.; Rinke, P.; Körzdörfer, T. Accurate Ionization Potentials and Electron Affinities of Acceptor Molecules II: Non-Empirically Tuned Long-Range Corrected Hybrid Functionals. *J. Chem. Theory Comput.* **2016**, *12*, 605−614.
(66) Knight, J. W.; Wang, X.; Gallandi, L.; Dolgounitcheva, O.; Ren, X.; Ortiz, J. V.; Rinke, P.; Körzdörfer, T.; Marom, N. Accurate Ionization Potentials and Electron Affinities of Acceptor Molecules III: A Benchmark of *GW* Methods. *J. Chem. Theory Comput.* **2016**, *12*, 615−626.
(67) Dolgounitcheva, O.; Díaz-Tinoco, M.; Zakrzewski, V. G.; Richard, R. M.; Marom, N.; Sherrill, C. D.; Ortiz, J. V. Accurate Ionization Potentials and Electron Affinities of Acceptor Molecules IV: Electron-Propagator Methods. *J. Chem. Theory Comput.* **2016**, *12*, 627−637.
(68) Jacquemin, D.; Duchemin, I.; Blase, X. Benchmarking the Bethe−Salpeter Formalism on a Standard Organic Molecular Set. *J. Chem. Theory Comput.* **2015**, *11*, 3290−3304.
(69) Lani, G.; Romaniello, P.; Reining, L. Approximations for Many-Body Green's Functions: Insights from the Fundamental Equations. *New J. Phys.* **2012**, *14*, 013056.
(70) Berger, J. A.; Romaniello, P.; Tandetzky, F.; Mendoza, B. S.; Brouder, C.; Reining, L. Solution to the Many-Body Problem in One Point. *New J. Phys.* **2014**, *16*, 113025.
(71) Berger, J. A.; Romaniello, P.; Tandetzky, F.; Mendoza, B. S.; Brouder, C.; Reining, L. Erratum: Solution to the Many-Body Problem in One Point (*New J. Phys.* 16 113025. *New J. Phys.* **2014**, *16*, 119601.
(72) Stan, A.; Romaniello, P.; Rigamonti, S.; Reining, L.; Berger, J. A. Unphysical and physical solutions in many-body theories: from weak to strong correlation. *New J. Phys.* **2015**, *17*, 093045.
(73) Tarantino, W.; Romaniello, P.; Berger, J. A.; Reining, L. Self-Consistent Dyson Equation and Self-Energy Functionals: An Analysis and Illustration on the Example of the Hubbard Atom. *Phys. Rev. B: Condens. Matter Mater. Phys.* **2017**, *96*, 045124.
(74) Tarantino, W.; Mendoza, B. S.; Romaniello, P.; Berger, J. A.; Reining, L. Many-body perturbation theory and non-perturbative approaches: screened interaction as the key ingredient. *J. Phys.: Condens. Matter* **2018**, *30*, 135602.
(75) Loos, P.-F.; Gill, P. M. W. Ground State of Two Electrons on a Sphere. *Phys. Rev. A: At., Mol., Opt. Phys.* **2009**, *79*, 062517.
(76) Loos, P.-F.; Gill, P. M. W. Two Electrons on a Hypersphere: A Quasiexactly Solvable Model. *Phys. Rev. Lett.* **2009**, *103*, 123008.
(77) Loos, P.-F.; Gill, P. M. A Tale of Two Electrons: Correlation at High Density. *Chem. Phys. Lett.* **2010**, *500*, 1−8.
(78) Loos, P.-F.; Gill, P. M. Excited States of Spherium. *Mol. Phys.* **2010**, *108*, 2527−2532.
(79) Seidl, M. Adiabatic Connection in Density-Functional Theory: Two Electrons on the Surface of a Sphere. *Phys. Rev. A: At., Mol., Opt. Phys.* **2007**, *75*, 062506.
(80) Schindlmayr, A. Analytic Evaluation of the Electronic Self-Energy in the G W Approximation for Two Electrons on a Sphere. *Phys. Rev. B: Condens. Matter Mater. Phys.* **2013**, *87*, 075104.
(81) Loos, P.-F.; Gill, P. M. W. Correlation Energy of Two Electrons in the High-Density Limit. *J. Chem. Phys.* **2009**, *131*, 241101.
(82) Loos, P.-F.; Gill, P. M. W. Invariance of the Correlation Energy at High Density and Large Dimension in Two-Electron Systems. *Phys. Rev. Lett.* **2010**, *105*, 113001.
(83) Loos, P.-F.; Gill, P. M. W. Thinking Outside the Box: The Uniform Electron Gas on a Hypersphere. *J. Chem. Phys.* **2011**, *135*, 214111.
(84) Loos, P.-F.; Gill, P. M. W. Exact Wave Functions of Two-Electron Quantum Rings. *Phys. Rev. Lett.* **2012**, *108*, 083002.
(85) Gill, P. M. W.; Loos, P.-F. Uniform Electron Gases. *Theor. Chem. Acc.* **2012**, *131*, 1069.
(86) Loos, P.-F. Understanding Excitons Using Spherical Geometry. *Phys. Lett. A* **2012**, *376*, 1997−2000.
(87) Loos, P.-F.; Bressanini, D. Nodal Surfaces and Interdimensional Degeneracies. *J. Chem. Phys.* **2015**, *142*, 214112.
(88) Loos, P.-F. Exchange Functionals Based on Finite Uniform Electron Gases. *J. Chem. Phys.* **2017**, *146*, 114108.
(89) Shishkin, M.; Kresse, G. Self-Consistent G W Calculations for Semiconductors and Insulators. *Phys. Rev. B: Condens. Matter Mater. Phys.* **2007**, *75*, 235102.
(90) Faleev, S. V.; van Schilfgaarde, M.; Kotani, T. All-Electron Self-Consistent G W Approximation: Application to Si, MnO, and NiO. *Phys. Rev. Lett.* **2004**, *93*, 126406.
(91) van Schilfgaarde, M.; Kotani, T.; Faleev, S. Quasiparticle Self-Consistent G W Theory. *Phys. Rev. Lett.* **2006**, *96*, 226402.
(92) Kotani, T.; van Schilfgaarde, M.; Faleev, S. V. Quasiparticle Self-Consistent G W Method: A Basis for the Independent-Particle Approximation. *Phys. Rev. B: Condens. Matter Mater. Phys.* **2007**, *76*, 165106.
(93) von Barth, U.; Holm, B. Self-Consistent GW 0 Results for the Electron Gas: Fixed Screened Potential W 0 within the Random-Phase Approximation. *Phys. Rev. B: Condens. Matter Mater. Phys.* **1996**, *54*, 8411.
(94) Hirata, S.; Hermes, M. R.; Simons, J.; Ortiz, J. V. General-Order Many-Body Green's Function Method. *J. Chem. Theory Comput.* **2015**, *11*, 1595−1606.
(95) Hirata, S.; Doran, A. E.; Knowles, P. J.; Ortiz, J. V. One-Particle Many-Body Green's Function Theory: Algebraic Recursive Definitions, Linked-Diagram Theorem, Irreducible-Diagram Theorem, and General-Order Algorithms. *J. Chem. Phys.* **2017**, *147*, 044108.
(96) Stefanucci, G.; van Leeuwen, R. *Nonequilibrium Many-Body Theory of Quantum Systems: A Modern Introduction*; Cambridge University Press: Cambridge, 2013.
(97) Ren, X.; Marom, N.; Caruso, F.; Scheffler, M.; Rinke, P. Beyond the G W Approximation: A Second-Order Screened Exchange Correction. *Phys. Rev. B: Condens. Matter Mater. Phys.* **2015**, *92*, 081104.
(98) Ren, X.; Rinke, P.; Joas, C.; Scheffler, M. Random-Phase Approximation and Its Applications in Computational Chemistry and Materials Science. *J. Mater. Sci.* **2012**, *47*, 7447−7471.

DOI: 10.1021/acs.jctc.8b00260
J. Chem. Theory Comput. 2018, 14, 3071−3082

(99) Romaniello, P.; Bechstedt, F.; Reining, L. Beyond the G W Approximation: Combining Correlation Channels. *Phys. Rev. B: Condens. Matter Mater. Phys.* **2012**, *85*, 155131.
(100) Aryasetiawan, F.; Sakuma, R.; Karlsson, K. G W Approximation with Self-Screening Correction. *Phys. Rev. B: Condens. Matter Mater. Phys.* **2012**, *85*, 035106.
(101) Wetherell, J.; Hodgson, M. J. P.; Godby, R. W. G W Self-Screening Error and Its Correction Using a Local Density Functional. *Phys. Rev. B: Condens. Matter Mater. Phys.* **2018**, *97*, 121102.
(102) Strinati, G. Application of the Green's Functions Method to the Study of the Optical Properties of Semiconductors. *Riv. Nuovo Cimento* **1988**, *11*, 1−86.
(103) Leng, X.; Jin, F.; Wei, M.; Ma, Y. GW Method and Bethe-Salpeter Equation for Calculating Electronic Excitations: GW Method and Bethe-Salpeter Equation. *Wiley Interdiscip. Rev. Comput. Mol. Sci.* **2016**, *6*, 532−550.
(104) Dreuw, A.; Wormit, M. The Algebraic Diagrammatic Construction Scheme for the Polarization Propagator for the Calculation of Excited States. *Wiley Interdiscip. Rev. Comput. Mol. Sci.* **2015**, *5*, 82−95.
(105) Dreuw, A.; Head-Gordon, M. Single-Reference Ab Initio Methods for the Calculation of Excited States of Large Molecules. *Chem. Rev.* **2005**, *105*, 4009−4037.
(106) Casida, M. E. Generalization of the Optimized-Effective-Potential Model to Include Electron Correlation: A Variational Derivation of the Sham-Schlüter Equation for the Exact Exchange-Correlation Potential. *Phys. Rev. A: At., Mol., Opt. Phys.* **1995**, *51*, 2005−2013.
(107) Dahlen, N. E.; van Leeuwen, R.; von Barth, U. Variational Energy Functionals of the Green Function and of the Density Tested on Molecules. *Phys. Rev. A: At., Mol., Opt. Phys.* **2006**, *73*, 012511.
(108) Furche, F. Developing the Random Phase Approximation into a Practical Post-Kohn−Sham Correlation Model. *J. Chem. Phys.* **2008**, *129*, 114105.
(109) Klein, A. Perturbation Theory for an Infinite Medium of Fermions. II. *Phys. Rev.* **1961**, *121*, 950−956.
(110) Luttinger, J. M.; Ward, J. C. Ground-State Energy of a Many-Fermion System. II. *Phys. Rev.* **1960**, *118*, 1417−1427.
(111) Galitskii, V.; Migdal, A. *Sov. Phys. JETP* **1958**, *7*, 96.
(112) Szabo, A.; Ostlund, N. S. *Modern Quantum Chemistry*; McGraw-Hill: New York, 1989.
(113) Pulay, P. Convergence Acceleration of Iterative Sequences. the Case of Scf Iteration. *Chem. Phys. Lett.* **1980**, *73*, 393−398.
(114) Pulay, P. ImprovedSCF Convergence Acceleration. *J. Comput. Chem.* **1982**, *3*, 556−560.
(115) Hernández, A. J.; Langhoff, P. W. On Rayleigh-Schrödinger and Green's-Function Calculations of Ionization Potentials and Electron Affinities. *Chem. Phys. Lett.* **1977**, *49*, 421−426.
(116) Casida, M. E.; Chong, D. P. Physical Interpretation and Assessment of the Coulomb-Hole and Screened-Exchange Approximation for Molecules. *Phys. Rev. A: At., Mol., Opt. Phys.* **1989**, *40*, 4837.
(117) Casida, M. E.; Chong, D. P. Simplified Green-Function Approximations: Further Assessment of a Polarization Model for Second-Order Calculation of Outer-Valence Ionization Potentials in Molecules. *Phys. Rev. A: At., Mol., Opt. Phys.* **1991**, *44*, 5773.
(118) Romaniello, P.; Guyot, S.; Reining, L. The Self-Energy beyond GW: Local and Nonlocal Vertex Corrections. *J. Chem. Phys.* **2009**, *131*, 154111.
(119) Almbladh, C.-O.; Barth, U. V.; Leeuwen, R. V. Variational Total Energies from Φ-and Ψ-Derivable Theories. *Int. J. Mod. Phys. B* **1999**, *13*, 535−541.
(120) Dahlen, N. E.; von Barth, U. Variational Energy Functionals Tested on Atoms. *Phys. Rev. B: Condens. Matter Mater. Phys.* **2004**, *69*, 195102.
(121) Dahlen, N. E.; von Barth, U. Variational Second-Order Møller−Plesset Theory Based on the Luttinger−Ward Functional. *J. Chem. Phys.* **2004**, *120*, 6826−6831.
(122) Dahlen, N. E.; van Leeuwen, R. Self-Consistent Solution of the Dyson Equation for Atoms and Molecules within a Conserving Approximation. *J. Chem. Phys.* **2005**, *122*, 164102.
(123) Dahlen, N. E.; Van Leeuwen, R.; Von Barth, U. Variational Energy Functionals of the Green Function Tested on Molecules. *Int. J. Quantum Chem.* **2005**, *101*, 512−519.

DOI: 10.1021/acs.jctc.8b00260
J. Chem. Theory Comput. 2018, 14, 3071−3082